JOURNAL OF GEOPHYSICAL RESEARCH, VOL. 103, NO. D24, PAGES 31,557–31,567, DECEMBER 27, 1998

Spreading and growth of contrails in a sheared environment

Eric J. Jensen,[1] Andrew S. Ackerman,[2] David E. Stevens,[3] Owen. B. Toon,[4] Patrick Minnis [5]

Abstract.

A case study of persistent contrail evolution in a sheared environment is simulated over time-scales of 15–180 min using a large-eddy simulation model with detailed microphysics. Model results are compared to satellite and in situ measurements of persistent contrails from the Subsonic Aircraft: Contrail and Cloud Effects Special Study (SUCCESS) experiment. In simulations with large ambient supersaturations and moderate wind shear, crystals with lengths > 200 μm are generated within 45 min by depositional growth. These crystals fall rapidly, and the contrail horizontal extent increases due to the wind shear. Strong radiative heating (with rates up to 10 K d^{-1}) drives a local updraft and lofts the contrail core several hundred meters. The observed rate of contrail spreading and maintenance of optical depths larger than 0.05 can be approximately explained simply by growth and precipitation of ice crystals nucleated during the initial contrail formation if the environmental humidity is very high (relative humidity with respect to ice > 125%). This result is consistent with observed high humidities in regions where persistent contrails formed during SUCCESS.

1. Introduction

Satellite observations of relatively young, linear contrails have shown that they cover only about 0.2 to 1% of the sky, even in regions with heavy air traffic [*Mannstein,* 1996; *Sassen,* 1997]. Hence, these readily identifiable contrails probably do not have a substantial impact on Earth's radiation budget or climate. However, recent satellite observations have documented cases in which contrails persisted for several hours and spread extensively to cover large areas [*Minnis et al.,* 1998]. These aged contrails eventually look very much like natural cirrus clouds, both in terms of their visual appearance and their microphysical composition [Spinhirne, personal communication]. Since these persistent contrails have long lifetimes and grow to cover large areas, they have the greatest potential for affecting regional or global climate. Hence, the key issues concerning the impact of contrails on climate are how often these persistent, spreading contrails form, and what environmental conditions are required for their formation.

The processes that drive contrail spreading are horizontal diffusion and vertical shear of the horizontal wind. In situ measurements of aged aircraft exhaust plumes have shown that wind shear typically dominates the horizontal spreading [*Schumann et al.,* 1995]. If a contrail remains confined to a relatively narrow vertical layer, then the potential for spreading by wind shear will be limited. However, precipitation of larger crystals in the contrail will increase the depth of the cloud. Hence, the spreading due to wind shear will likely depend upon the microphysical evolution of the contrail in addition to the magnitude of the wind shear.

In the initial stage of contrail formation, large numbers of ice crystals are nucleated. The simplest conceptual model of contrail evolution is that this initial collection of ice crystals just disperses and the crystals grow. In this scenario, the ice crystal number density will continue to decrease with time, but the total number of crystals per unit distance along the flight path (contrail axis) will remain constant. Recent remote sensing measurements of contrails with different ages showed that the number of crystals per unit distance along the flight path remained roughly constant as the contrails aged [*Spinhirne et al.,* 1998]. Satellite observations have shown that the optical depth of persistent contrails remains relatively large (above about 0.05–0.1) as they

[1]NASA Ames Research Center, Moffett Field, California.

[2]University of Colorado, Department of Atmospheric and Ocean Sciences, Boulder, Colorado.

[3]Lawrence Livermore National Laboratory, Livermore, California.

[4]Laboratory for Atmospheric and Space Physics, Department of Atmospheric and Oceanic Science, University of Colorado, Boulder, Colorado.

[5]NASA Langley Research Center, Hampton, Virginia.

Copyright 1998 by the American Geophysical Union.

Paper number 98JD02594.
0148-0227/98/98JD-02594$09.00

spread for several hours [*Minnis et al.*, 1998]. A fundamental question is whether the growth of ice crystals in a spreading contrail is sufficient to maintain the optical depth as observed despite the decreasing crystal number density. The lidar data presented by *Spinhirne et al.* [1998] suggest that the crystal growth does indeed account for the optical depth of aged contrails. An alternate explanation for the observed maintenance of optical depth is that new ice crystals are nucleated as the contrail evolves.

Another interesting phenomenon occasionally observed is the formation of precipitation streamers out of contrails. *Heymsfield et al.* [1998] speculated that ice crystals large enough to precipitate are generated near the boundaries of the contrail where ice crystals are exposed to significant supersaturations (within the contrail, supersaturations are expected to be suppressed by crystal growth). However, it is not clear how large the ambient supersaturation with respect to ice must be for these large crystals to form.

To address these issues, we use a large-eddy simulation (LES) model to simulate the evolution of contrails on time-scales ranging from about 15 min to a few hours. Past modeling studies of contrails have focused on the first 30 min of contrail evolution [*Gierens*, 1996; *Chlond*, 1998]. The model includes a detailed, size-resolving microphysics treatment and a radiative transfer code. We use model simulations to evaluate the processes responsible for contrail spreading, and to determine the environmental conditions required for contrail persistence. Specifically, we simulate the contrail generated on May 12, 1996 during the Subsonic Aircraft: Contrail and Cloud Effects Special Study (SUCCESS). We compare the model results with satellite observations of contrail evolution.

2. Observations of Persistent Contrails

On two occasions, persistent contrails have been sampled in situ with aircraft instrumentation [*Knollenberg*, 1972; *Heymsfield et al.*, 1998]. These measurements showed that relatively large (lengths of a few hundred microns), precipitating ice crystals developed within about 15–45 min contrail age. Also, measurements from SUCCESS showed that contrails persist longer than a few minutes only if they form in regions with large-scale supersaturation with respect to ice [*Jensen et al.*, 1998a]. *Minnis et al.* [1998] described three cases of contrails that persisted for hours and spread to cover areas larger than 10^3 km^2. The optical depths of these contrails were determined from GOES satellite measurements. Over time-scales of several hours, the visible optical depths of these contrails remained larger than about 0.2.

For detailed comparison with simulations, we will focus here on the persistent contrail sampled extensively on May 12, 1996, during SUCCESS. From about 2240 to 2330 UT, the NASA DC-8 flew in a racetrack pattern off the coast of northern California. During repeated loops through the pattern, it was visually apparent that the aircraft had generated a persistent, growing contrail. The racetrack shaped contrail was visible in 4-km resolution GOES-9 satellite images by 2345 UT. The satellite images showed that the cross-track width of the contrail was about 5 km at 30 min contrail age and 10 km at 90 min contrail age (see Plate 1). Repeated passes through the contrail with the DC-8 showed that large crystals were developing in the contrail, with the largest crystals near the contrail edges. In situ water vapor measurements showed that the contrail was generated in an extensive region with large supersaturations with respect to ice (relative humidities with respect to ice as high as 150%).

During the time period while the DC-8 was generating and sampling this contrail (about 2300 – 2342 UT), the aircraft flew in and out of the contrail and occasionally descended below the contrail. Plate 2 shows height profiles of temperature, wind velocity, and relative humidity with respect to ice (RHI) measured during this time period (see *Heymsfield et al.* [1998] for details of the instruments used). The temperature lapse rate was slightly stable (9.5 K km^{-1}) and did not vary much with horizontal location and time. The vertical shear of the horizontal wind perpendicular to the racetrack legs was about 5–10 m s^{-1} km^{-1} in the altitude range where the contrail formed (10–10.5 km). Throughout the region, the ambient air was highly supersaturated with respect to ice.

3. Simulations of Contrail Spreading

3.1 Model Description

We will show that the radiative heating in the contrail substantially affects the dynamics on time-scales longer than about 15–30 min. As a result, these contrail simulations require inclusion of interactive microphysics, radiation, and dynamics. For this purpose, we use an LES simulation model coupled to a detailed ice microphysics model. The LES model HUSCI [*Stevens and Bretherton*, 1996] is used in this study primarily as a two-dimensional eddy-resolving model. The model integrates the anelastic momentum equations [*Ogura and Phillips*, 1962] using a forward-in-time solver with a second-order, conservative advection scheme that is both efficient and stable. A first-order subgrid-scale turbulence closure modified to account for the effects of evaporation is used. We use a 2-D grid domain with a vertical depth of 5 km and a width of 20 km oriented perpendicular to the contrail axis. A vertical grid spacing of 20 m and a horizontal grid spacing of 40 m are used. Periodic boundary conditions are used at the horizontal boundaries, and rigid boundary conditions are used at the vertical boundaries.

The detailed microphysical model that is coupled to the LES model has been used to study a variety of cir-

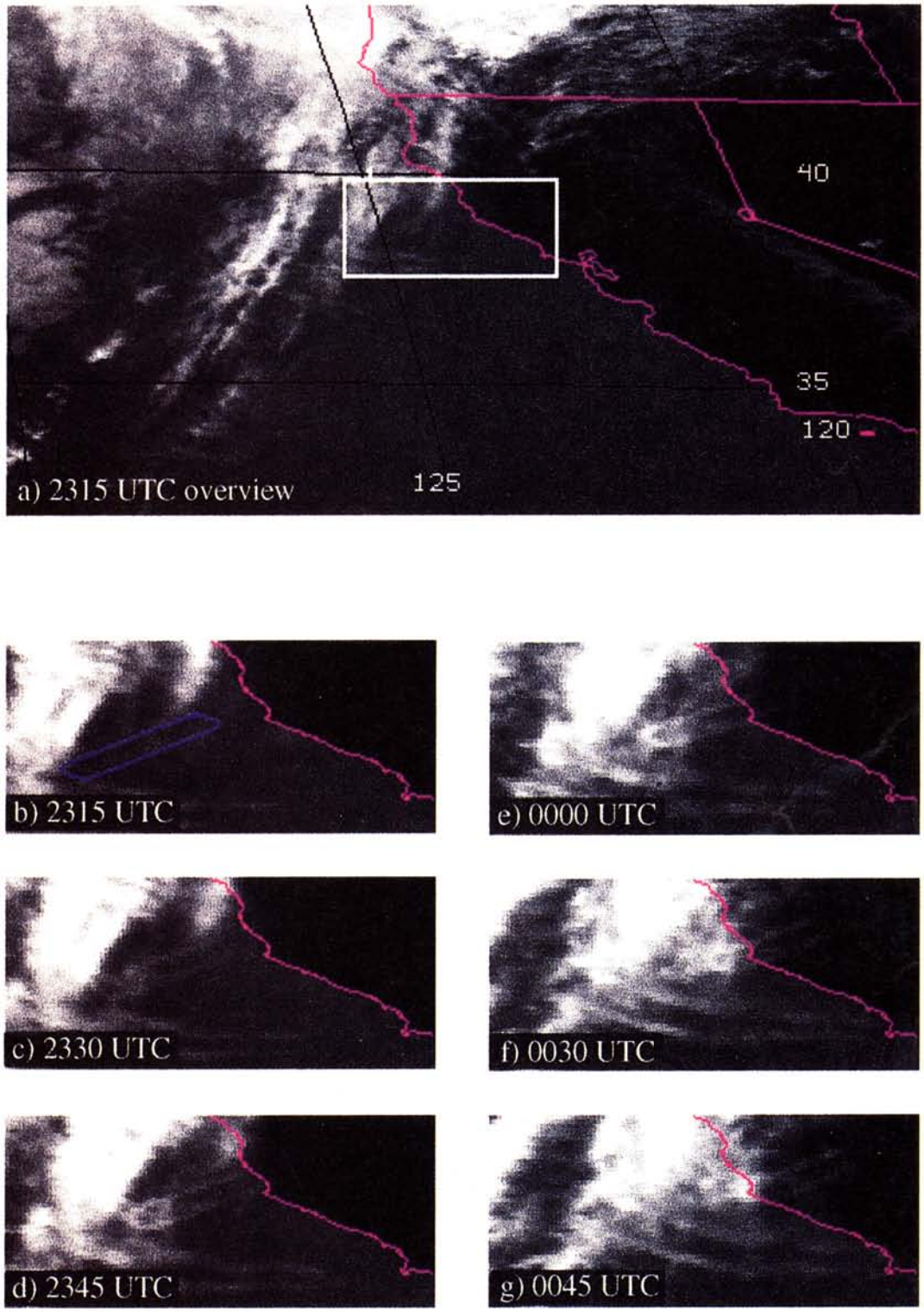

Plate 1. Sequence of GOES-9 10.8 μm satellite images showing the evolution of the DC-8 contrail generated on May 12, 1996. The DC-8 flight path is the blue oval shown in (Plate 1b).

rus cloud types and cirrus processes [e.g., *Jensen et al.*, 1998b]. Processes such as ice nucleation, ice crystal depositional growth, coagulation, sedimentation, and sublimation can be simulated with this model. For these simulations, we include only ice crystals, with 25 crystal size bins spanning the equivalent-volume radius range from 0.5–350 μm. Since we are focusing here on the issue of whether dispersion of the contrail alone can explain the observations, we have not included nucleation of new ice crystals in the simulation. We use the two-stream radiative transfer model described by *Toon et al.* [1989]. This model includes 26 bands at solar

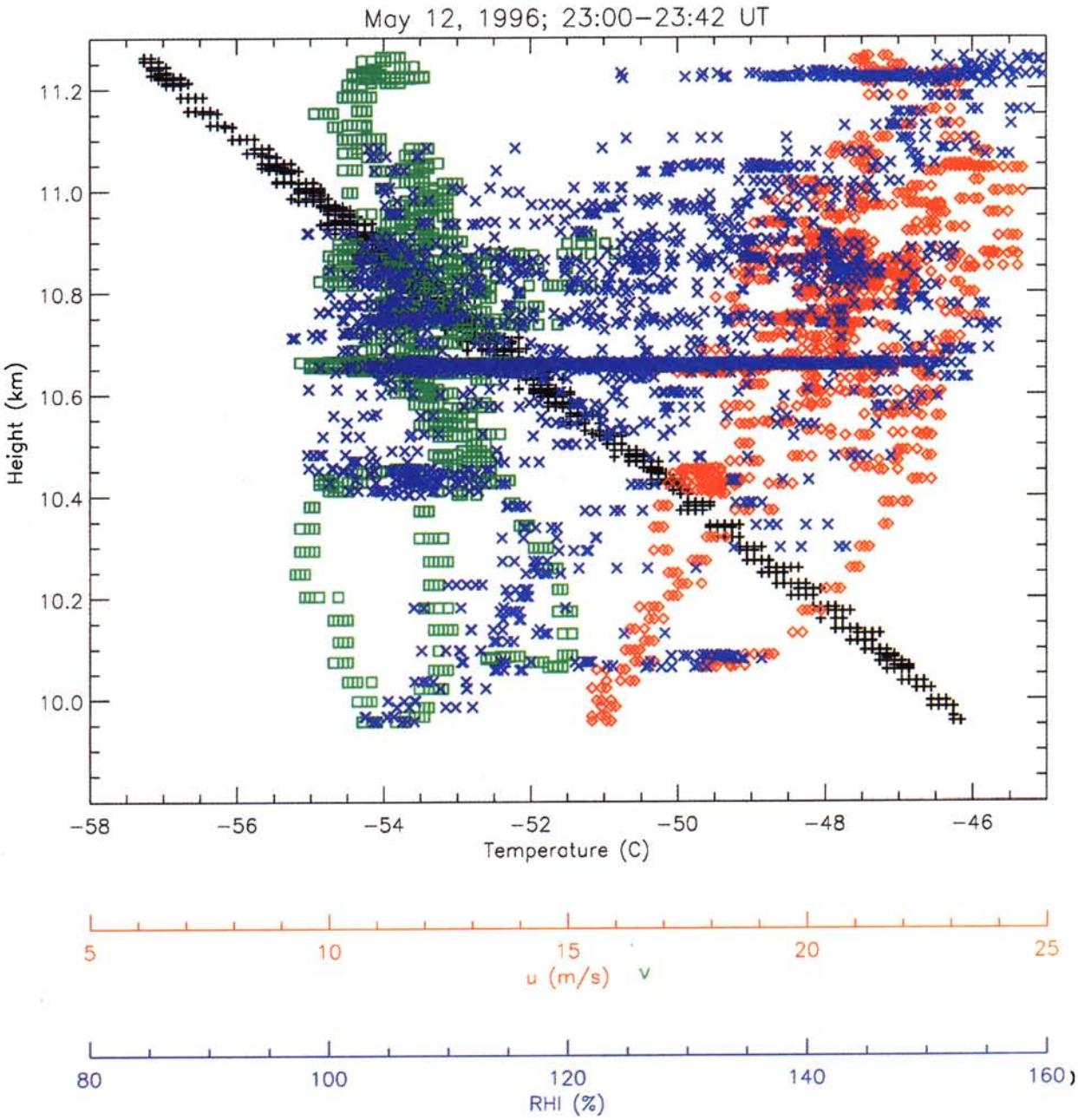

Plate 2. Height profiles of temperature (black), horizontal wind speeds (red and green), and RHI (blue). The measurements were made with instruments on the DC-8 from 2300 – 2342 UT, May 12, 1996, while the aircraft was flying in the region where the contrail shown in Plate 1 was generated.

wavelengths and 18 bands at infrared wavelengths. Ice crystal single-scattering properties are calculated with a Mie scattering code. For the radiation calculations, we include 10 layers which extend from the surface up to the base of the contrail model domain (8 km). The assumed surface temperature and emissivity are 287.6 K and 1.0. Water vapor, carbon dioxide, and ozone concentrations below the contrail model domain are specified based on the midlatitude summer U.S. Standard Atmosphere. The radiation calculations also include a layer above the contrail model domain to account for the impact of stratospheric ozone on radiative fluxes.

We initialize our simulations with a representation of a mature contrail approximately 15 min old. At this age, contrails are typically somewhat flattened, with a horizontal width of about 1 km and a vertical thickness of about 200 m [*Freudenthaler et al.*, 1995; *Gierens*, 1996]. We use a 2-D Gaussian distribution to represent the initial contrail structure, with horizontal and vertical standard deviations of 400 m and 100 m, respectively. To match the conditions observed on May 12, 1996, the contrail is initially centered at at 10.5 km. The initial ice crystal size distribution used is a lognormal with a number density of 20 cm^{-3} at the center

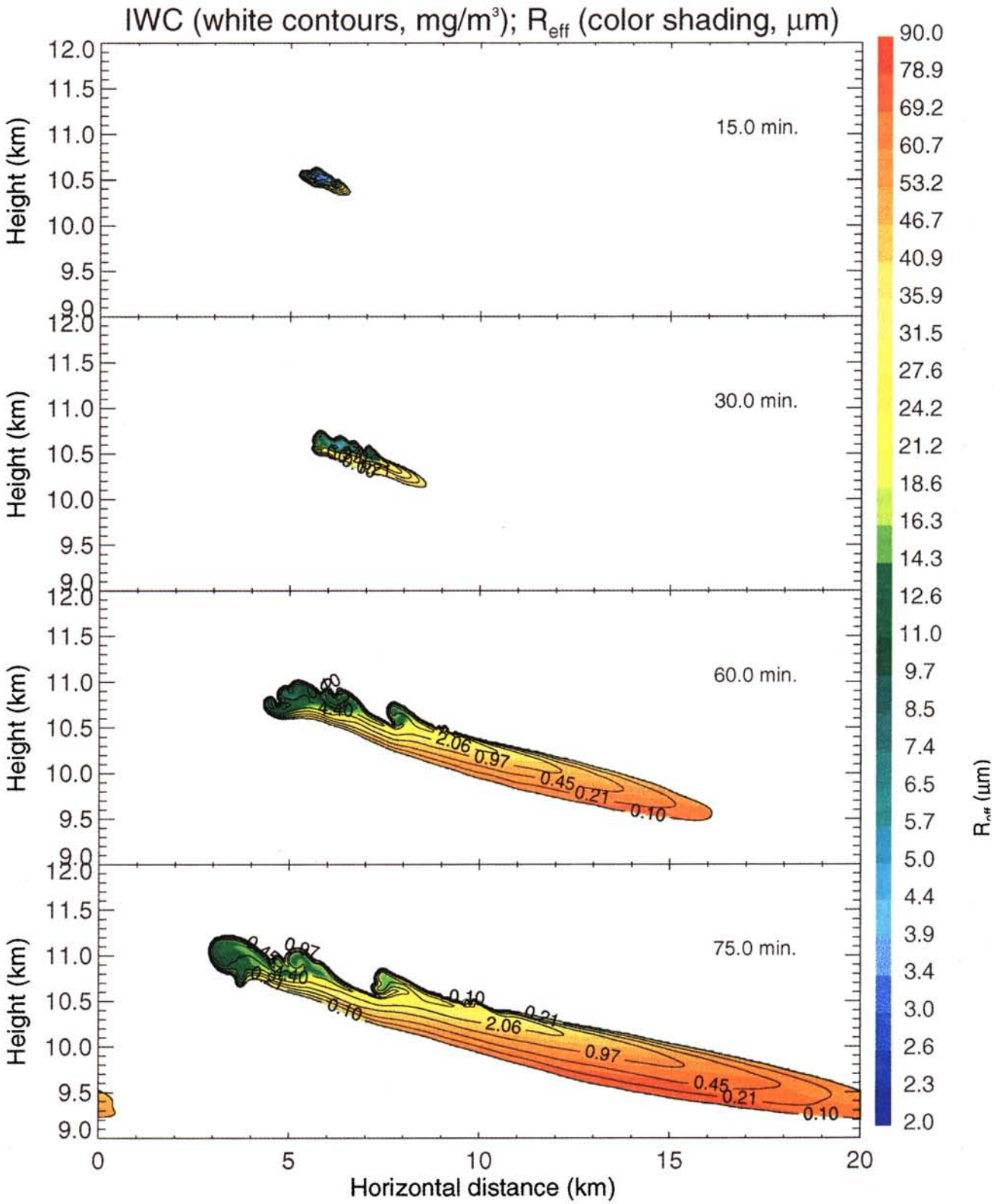

Plate 3. Contours of ice water content plotted versus cross-track horizontal distance and height at four different times in the baseline simulation. The color shading shows the effective radius of the ice crystals. The sorting of crystal size with height as well as the contrail spreading are evident.

of the contrail, a mode radius of 2 μm, and a geometric standard deviation of 1.3 throughout the contrail. The zenith visible optical depth of this contrail is 0.1 at its center.

We specify the model atmosphere based on the DC-8 measurements shown in Plate 2. The lapse rate assumed is 9.5 K km^{-1}, and the horizontal shear of the vertical wind is 6 m s^{-1} km^{-1}. The corresponding gradient Richardson number is 0.59; i.e., the vertical structure is slightly stable. For our baseline simulation, we use an ambient RHI of 125% throughout the domain, and an initial random temperature perturbation of 0.25 K is applied.

3.2 Model results

Plate 3 shows the evolution of the contrail spatial structure in the baseline simulation. Contours of ice water content and effective radius are plotted at four different times. Due to the ambient supersaturation, ice crystals near the edges of the contrail grow rapidly. Ice crystals with lengths larger than 100 and 200 μm are generated within 30 and 45 min of the beginning of the simulation, respectively. The larger ice crystals fall most rapidly, resulting in a size sorting with height in the contrail. The combination of crystal sedimentation, vertical motions, and wind shear results in a substantial horizontal stretching of the contrail.

The maximum ice crystal number density falls from the initial value of 20 cm^{-3} to about 3 cm^{-3} at 75 min and 0.8 cm^{-3} at 3 hours. Hence, the ice crystal number density in the contrail core substantially decreases due to dispersion and precipitation of larger crystals; however, an ample supply of crystals still remains for the contrail to be visible. In other words, it is plausible that the contrail optical depth can be maintained without nucleation of new ice crystals.

Plate 4 shows the spatial distributions of ice water content, relative humidity, heating rate, and vertical wind speed at 45 min into the simulation. The assumed initial random temperature perturbation is included to represent the possibility of transient turbulence. Due to the slightly stable thermal structure, the random temperature perturbations lead to vertical wind speeds of only a few mm-s^{-1} and RHI perturbations of less than 5%. Inclusion of the random temperature perturbations has very little impact on the contrail evolution. In a simulation with no temperature perturbations, the contrail evolution is essentially identical to our baseline simulation with 0.25 K temperature perturbations.

The radiative heating rate in the contrail is as large as 10 K d^{-1} early in the simulation. The heating is dominated by absorption of upwelling infrared radiation. The contrail absorbs upwelling radiation emitted by the warm surface below, and radiative emission from the contrail is limited by its low temperature. The net result is deposition of radiative energy in the contrail. Latent heating is negligible. The heating in the contrail drives a local updraft with peak vertical wind speeds up to 5 cm s^{-1}. As a result, the core of the contrail is lofted several hundred meters during the first hour of the simulation. The RHI field shown in Plate 4 shows that a local enhancement in the relative humidity is driven by the updraft. Within the core of the heating at about 10.7 km, the RHI is actually suppressed due to a slight increase in the temperature. However, due to continuity, the updraft extends through a larger vertical extent than the heating itself. Hence, just above the contrail core, the vertical motion drives adiabatic cooling and an increase in humidity. Relative humidities with respect to ice as large as 150% are generated within 1 hour of the beginning of the simulation. These RHI peaks would probably drive nucleation of new ice crystals. (As discussed above, we have not included ice nucleation in these simulations.)

Heymsfield et al. [1998] reported that the contrail sampled on May 12, 1996, ascended at a rate of about 10 cm s^{-1}. Our simulation suggests that this ascent may have been due to lofting of the radiatively heated contrail. The lofting rate in our simulation is smaller (about 5 cm s^{-1}); however, as described below, the vertical motion driven by heating is strongly sensitive to the assumed temperature lapse rate.

Plate 5 shows the zenith infrared optical depth of the contrail versus time and horizontal distance (perpendicular to the contrail axis). After about 1 hour, the peak optical depth has increased from 0.1 to about 0.3, and the width of the contrail with optical depth larger than 0.05 has increased from 1 km to about 4 km. As discussed above, the GOES-9 images indicated that the contrail width increased from about 2 to 10 km at contrail ages of 30–90 min.

We have run numerous sensitivity tests varying parameters such as the initial ice crystal size distribution, the ambient RHI, and the temperature lapse rate. Results are summarized in Table 1. The sensitivity of the contrail spreading to ambient humidity is shown in Figure 1, and the variation of the contrail width at 60 min is plotted versus ambient RHI in Figure 2. If the ambient air is only slightly supersaturated with respect to ice, then the contrail ice crystals do not grow rapidly, little or no precipitation occurs, and the contrail does not spread substantially. Only if the ambient RHI is very large (> 125%) does the contrail spread as fast as indicated by the observations.

To evaluate the role of crystal sedimentation in the contrail evolution, we have run a simulation with the fallspeeds set to 0 (case I). The width of the contrail at 60 min (3.7 km) was somewhat less than the width in the baseline simulation (4.2 km). Substantial spreading still occurs even without sedimentation due to the vertical motions driven by radiative heating. These motions disperse the contrail through a depth of several hundred meters and allow the wind shear to spread the contrail. If both radiative heating and sedimentation are shut off, then the contrail spreading is very limited.

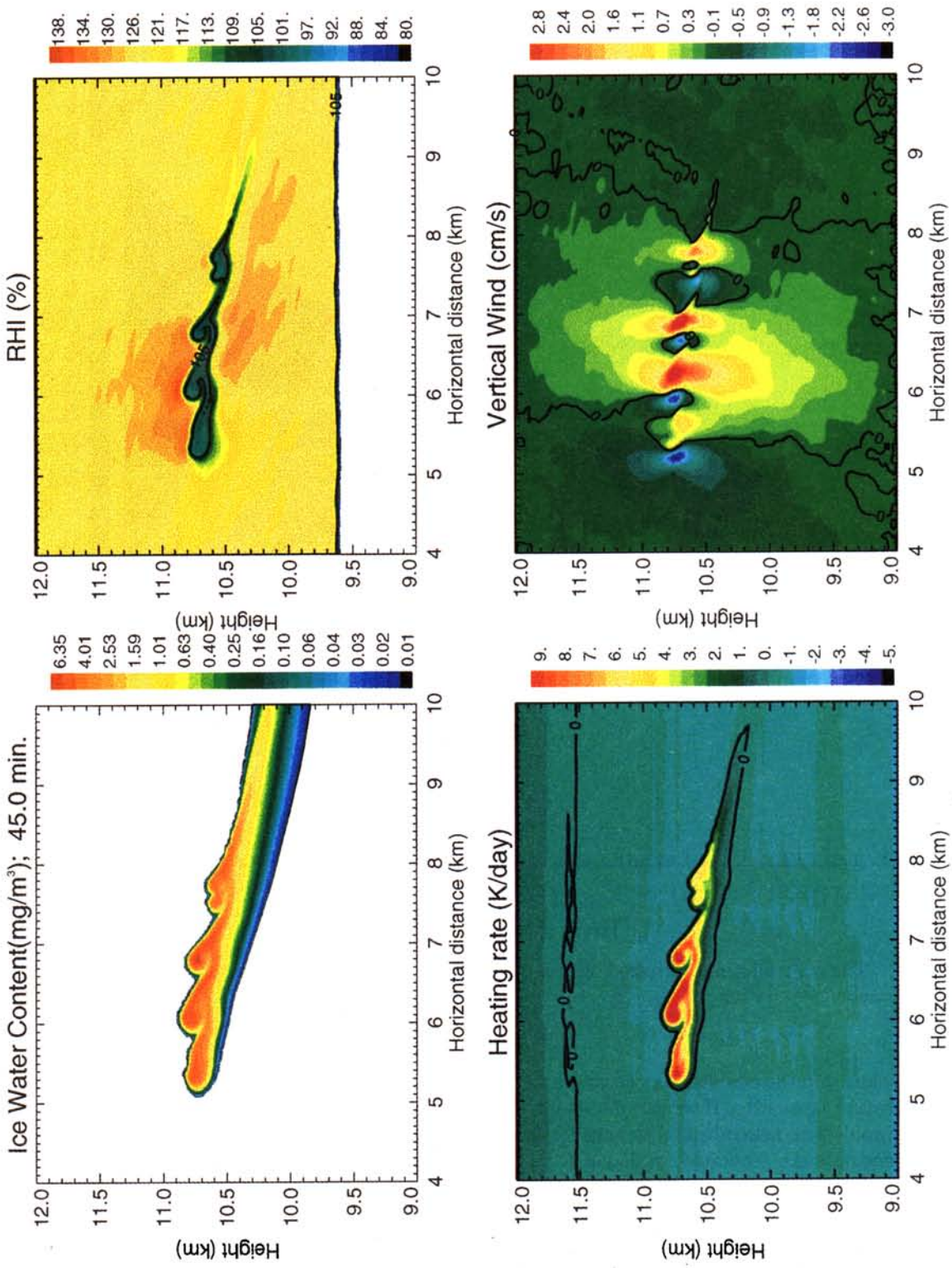

Plate 4. The spatial distributions of ice water content, relative humidity, heating rate, and vertical wind speed are shown at 45 min into the baseline simulation. Radiative heating drives an updraft in the vicinity of the contrail core. This updraft causes cooling and increased relative humidities above and below the contrail.

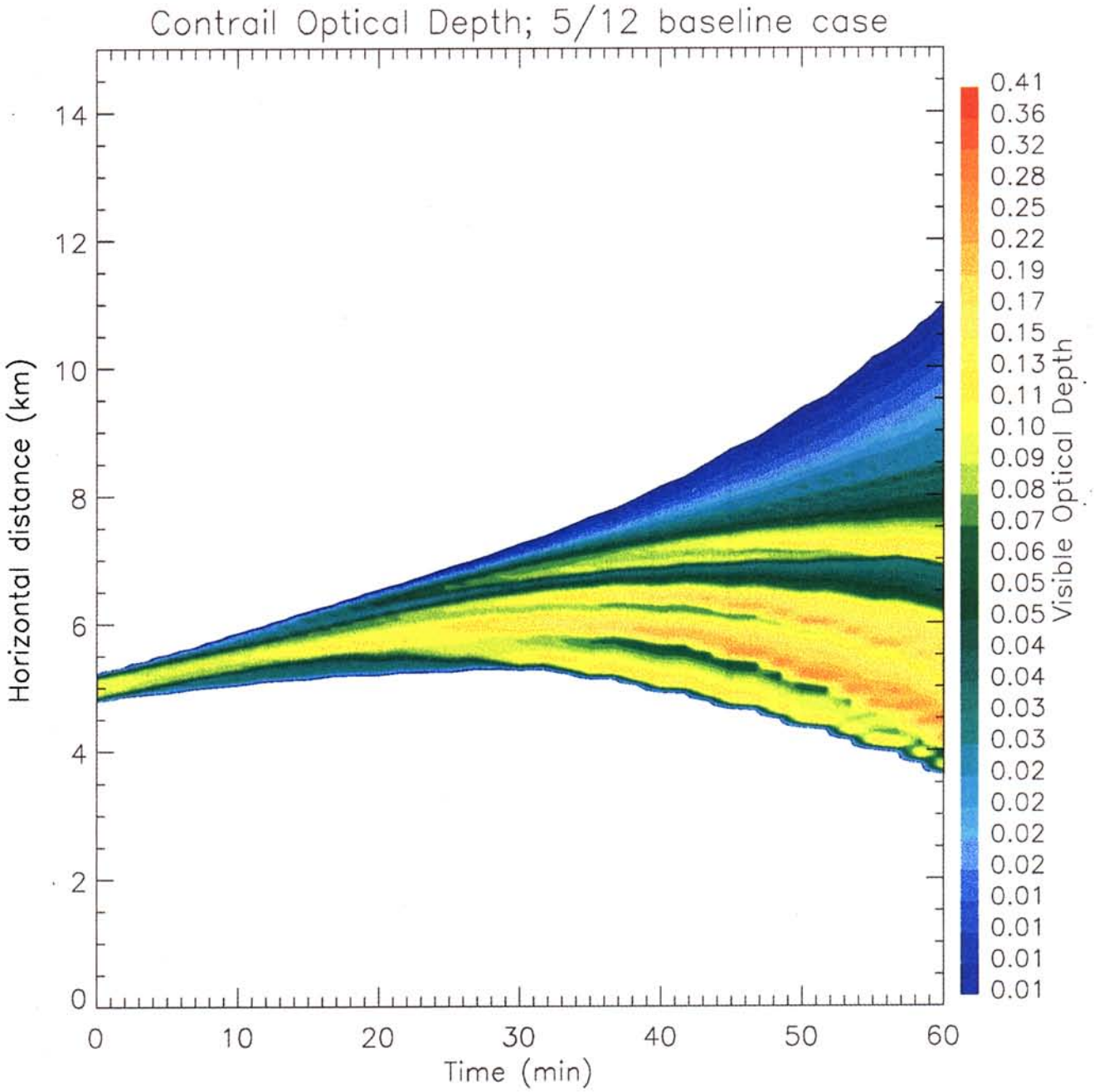

Plate 5. The contrail zenith infrared optical depth plotted versus time and cross-track distance for the baseline simulation.

The contrail evolution in the model is very sensitive to the initial temperature lapse rate. If we assume an initial temperature profile with neutral stability, then large updrafts and downdrafts are generated (> 25 cm s^{-1}), and the contrail structure is much more complicated (case E). The larger wind perturbations drive peak ice supersaturations in excess of 200%, which would no doubt drive nucleation of new ice crystals. Even in regions of the model domain away from the contrail, substantial updrafts are driven by the random temperature perturbation. If we use a strongly stable temperature profile, then the contrail heating does not drive substantial vertical motions, and the contrail peak optical depth decreases monotonically with time (case F).

During the May 12 flight, the DC-8 looped around the racetrack pattern 2–3 times. It is possible that the width of the contrail observed later in its lifetime was partly due to the DC-8 flying alongside the contrail made during a previous loop. To evaluate this possibility, we have run a simulation using an initial contrail twice as wide as in our baseline simulation (case J). However, at 60 min the contrail in this case is only slightly wider than in the baseline simulation.

We have also run a few 3-D simulations to make sure

Table 1. Sensitivity Test Results at 60 min

Case	Notes	IWC_{max},[a] mg m^{-3}	τ_{max}	τ_{ave}	Width,[b] km
A. Baseline[c]	RHI=125%	7.3	0.27	0.030	4.2
B. High RHI	RHI=145%	12.5	0.41	0.053	5.6
C. Low RHI	RHI=105%	5.5	0.21	0.010	1.2
D. Subsaturated	RHI=95%	3.1	0.096	0.004	0.68
E. Neutral stability	N=0	10.5	0.34	0.043	5.0
F. Strong stability	N=0.018	4.7	0.088	0.013	2.8
G. Small crystals	r_e=1 μm, N_{ice}=75 cm^{-3}	8.4	0.44	0.049	5.0
H. Large crystals	r_e=8 μm, N_{ice}=1.35 cm^{-3}	7.9	0.15	0.012	0.76
I. No Sedimentation	v_{fall}=0	7.5	0.24	0.024	3.7
J. Double-wide	σ_x=800 m	8.12	0.46	0.046	5.0

[a]The maximum contrail ice water content is given.
[b]Horizontal cross-plume width of contrail where $\tau \geq 0.05$.
[c]r_e=2 μm, N_{ice}=20 cm^{-3}, Brunt-Väisälä frequency=N=4.6x10^{-3} s^{-1}.

the 2-D simulations are not providing an unrealistic representation of the lofting driven by radiative heating. For the 3-D simulations, we include 15 planes along the contrail axis (corresponding to a horizontal distance of 600 m). Periodic boundary conditions are used along the new axis. In the 3-D simulations, some cellular structure is apparent along the contrail axis, but the updraft velocities are similar to those in the 2-D simulations. The updraft speeds in the contrail core at 45 min simulation time range from 3.6–8.8 cm s^{-1} along the contrail axis; in the 2-D simulation, the updraft speed in the contrail core at 45 min is 4.4 cm s^{-1}.

Simulations were run with initial ice crystal mode radii of 1, 4, and 8 μm rather than 2 μm used in the baseline simulation. The simulations with 1 and 8 μm effective radii correspond to cases G and H in Table 1. The initial ice crystal number densities were also adjusted, such that the initial peak visible optical depth in each of these contrails is 0.1. The contrail width at 60 min is plotted versus the initial crystal mode radius in Figure 2. In the small crystal simulations, rapid crystal growth near the boundary of the contrail results in

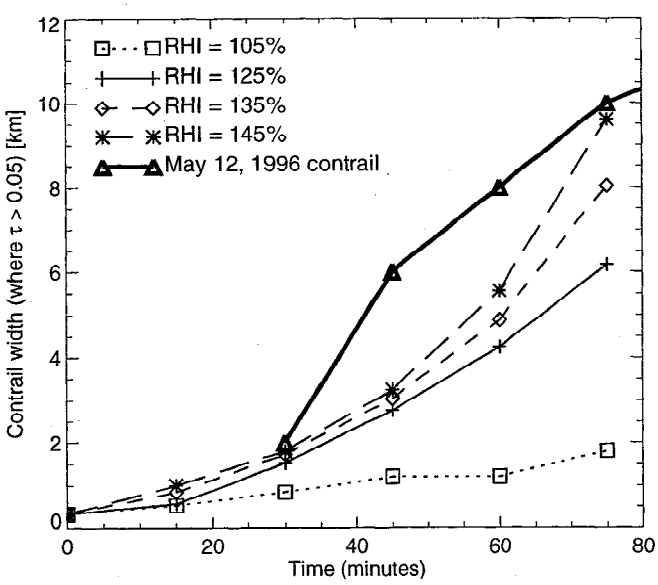

Figure 1. The contrail width plotted versus time for simulations with ambient RHI of 105, 125, 135, and 145%. The width is defined as the distance over which the optical depth is at least 0.05. The thick lines connecting the triangles are the cross-track width of the contrail determined from analysis of the GOES-9 visible images. The optical depth threshold for this analysis was about 0.05–0.1. For RHI $\leq$ 125%, the simulated contrail does not spread as fast as the observations indicate.

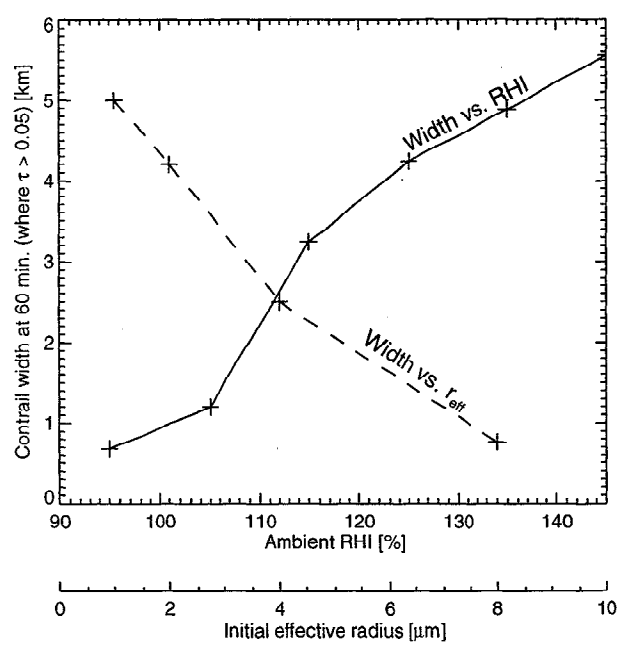

Figure 2. The contrail width at 60 min plotted versus the ambient RHI (solid curve) and versus the initial ice crystal effective radius (dashed curve). The ice crystal number densities were adjusted in these simulations such that the initial contrail optical depth is the same in all simulations (see Table 1).

substantial increase in the contrail optical depth (to a peak value of 0.44). After 60 min in this simulation, the width of the contrail (with optical depth greater than 0.05) has increased to 5 km. In the simulation initialized with 8 μm crystals, a reduced potential for crystal growth and the reduced crystal number density resulted in the contrail optical depth and width increasing much more slowly than in the baseline simulation.

4. Discussion

Our simulations for contrail ages up to 3 hours suggest that the depositional growth of ice crystals and contrail spreading due to shear could be the dominant mechanism controlling contrail growth. Secondary nucleation of new ice crystals in contrail updrafts is not necessarily required to explain the observed contrail spreading and optical depth on May 12, 1996. However, this scenario is consistent with the observations only if the ambient RHI is relatively high (> 125%). Also, the horizontal spreading occurs primarily as a result of ice crystal precipitation, vertical mixing driven by radiative heating, and the vertical shear of the horizontal wind. Hence, the simulated contrails span 4–5 km in the vertical by the time they are about 90 min old. Streamers originating from persistent contrails have been observed to extend several km below the contrails [*Konrad and Howard,* 1974].

As observed, growth of crystals large enough (lengths > 100 μm) to precipitate out of the contrails occurs in the simulation within about 30 min if the ambient RHI is high. In these simulations, the large crystals exist primarily downwind of and below the contrail core.

Under conditions with weak stability, radiative heating can loft the contrail and generate supersaturations which might lead to secondary nucleation of ice crystals. An interesting issue for a future study would be to examine how important such secondary ice nucleation is for the contrail radiative properties. The contrail lofting also raises the possibility that contrails formed in slightly subsaturated conditions might persist. However, the width of these contrails would remain somewhat limited, and they might not remain visible very long.

It should be emphasized here that this analysis is a case study of contrail evolution for a particular set of environmental conditions. The crystal growth, contrail optical properties, contrail dynamics, and generation of precipitation no doubt depend strongly on the contrail temperature, wind shear, and other conditions. In particular, the contrail radiative heating is sensitive to several environmental factors such as surface temperature, the presence of clouds below the contrail, the contrail temperature, the contrail ice water content, and the contrail spatial structure. Contrails formed at lower heights and higher temperatures would have higher ice water contents and higher optical depths [*Gierens,* 1996], which would tend to result in higher heating rates. However, the contrail-surface temperature difference would be smaller for the warmer contrails tending to limit the infrared absorption. We plan to investigate these sensitivities in a future study.

Acknowledgments. This research was supported by NASA's Subsonic Assessment Program, directed by Howard Wesoky. We are also grateful to Louis Nguyen of Analytical Services and Materials, Inc., Hampton, Virginia, for providing the satellite imagery.

References

Appleman, H., The formation of exhaust contrails by jet aircraft, *Bull. Am. Meteorol. Soc., 34,* 14–20, 1953.

Chlond, A., Large-eddy simulations of contrails, *J. Atmos. Sci., 55,* 796–819, 1998.

Collins, J. E., Jr., G. W. Sachse, L. G. Burney, and L. O. Wade, A novel external path water vapor sensor, paper presented at the NASA Atmospheric Effects of Aviation Program 5th annual meeting, Virginia Beach, April 23–28, 1995.

Freudenthaler V., F. Homburg, and H. Jäger, Contrail observations by ground-based scanning lidar: cross-sectional growth. *Geophys. Res. Lett.,* 22, 3501-3504. 1995.

Gierens, K., Numerical simulations of persistent contrails, *J. Atmos. Sci., 54,* 3333, 1996.

Heymsfield, A. J., and L. M. Miloshevich, Upper tropospheric relative humidity observations and implications for initiation of cirrus clouds, *Geophys. Res. Lett., 25,* 1343, 1998.

Heymsfield, A. J., R. P. Lawson, and G. W. Sachse, Growth of ice crystals in a precipitating contrail, *Geophys. Res. Lett., 25,* 1335, 1998.

Jensen, E. J., and O. B. Toon, Ice nucleation in the upper troposphere: Sensitivity to aerosol number density, temperature, and cooling rate, *Geophys. Res. Lett., 21,* 2019, 1994.

Jensen, E. J., O. B. Toon, S. Kinne, G. W. Sachse, B. Anderson, K. R. Chan, C. Twohy, B. Gandrud, A. Heymsfield, and R. C. Miake-Lye, Environmental conditions required for contrail formation and persistence, *J. Geophys. Res., 103,* 3929–3936, 1998a.

Jensen, E. J., et al., Ice nucleation in upper troposphere wave-clouds observed during SUCCESS, *Geophys. Res. Lett., 25,* 1363, 1998b.

Kärcher, B., Th. Peter, U. M. Biemann, and U. Schumann, The initial composition of jet condensation trails, *J. Atmos. Sci., 53,* 3066, 1996.

Knollenberg, R. G., Measurements of the growth of the ice budget in a persisting contrail, *J. Atmos. Sci., 29,* 1367, 1972.

Konrad, T. G., and J. C. Howard, Multiple contrail streamers observed by radar, *J. Appl. Meteorol., 13,* 563–572, 1974.

Liou, K.-N., S. C. Ou, and C. Koenig, An investigation on the climatic effect of contrail cirrus, *Lecture Notes Eng., 60,* 138-153, 1990.

Mannstein, H., Contrail observations from space using NOAA-AVHRR data, in *Proceedings International Colloquium, Impact of Aircraft Emissions upon the Atmosphere,* Off. Natl. d'Etudes et de Recl. Aeros., , Paris, pp. 427-431, 1996.

Minnis, P., D. F. Young, D. P. Gerber, L. Nguyen, W. L. Smith, Jr., and R. Palikonda, Transformation of contrails into cirrus clouds during SUCCESS, *Geophys. Res. Lett., 25,* 1157, 1998.

Ogura, Y., and N. Phillips, Scale analysis of deep and shal-

low convection in the atmosphere, *J. Atmos. Sci., 19,* 173–179, 1962.

Sassen, K., Contrail-cirrus and their potential for climate change, *Bull. Am. Meteorol. Soc., 78,* 1885–1903, 1997.

Schumann, U., On conditions for contrail formation from aircraft exhausts, *Meteorol. Z., 5,* 4–23, 1996.

Schumann, U., et al., Estimation of diffusion parameters of aircraft exhaust plumes near the tropopause from nitric oxide and turbulence measurements, *J. Geophys. Res., 100,* 14,147–14,162, 1995.

Schumann, U., et al., In situ observations of particles in jet aircraft exhaust and contrails for different sulfur containing fuels, *J. Geophys. Res., 101,* 6853, 1996.

Spinhirne, J. D., W. D. Hart, and D. P. Duda, Evolution of the morphology and microphysics of contrail cirrus from airborne remote sensing, *Geophys. Res. Lett., 25,* 1153, 1998.

Stevens, D. E., and C. S. Bretherton, A forward-in-time advection scheme and adaptive multilevel flow solver for nearly incompressible atmospheric flow, *J. Comput. Phys.,* 129, 284–295, 1996.

Toon, O. B., C. P. McKay, T. P. Ackerman, and K. Santhaman, Rapid calculation of radiative heating and photodissociation rates in inhomogeneous multiple scattering atmospheres, *J. Geophys. Res., 94,* 16.287–16,301, 1989.

E. J. Jensen and A. S. Ackerman, NASA Ames Research Center, MS 245-4, Moffett Field, CA 94035. (ejensen@sky.arc.nasa.gov)

D. E. Stevens, Lawrence Livermore National Laboratory, Atmospheric Sciences division, Livermore, CA 94550. (stevens@mothra.lbl.gov)

O. B. Toon, University of Colorado, LASP, Campus Box 392, Boulder, CO, 80309. (toon@lasp.colorado.edu)

P. Minnis, NASA Langley Research Center, MS 420, Hampton, VA 23681-0001. (p.minnis@larc.nasa.gov)

(Received January 31, 1998; revised July 28, 1998; accepted July 30, 1998.)